AD_____

Award Number: W81XWH-10-1-0173

TITLE: Tissue and Metabolomic Biomarkers of Recurrent Renal Cell Carcinoma

PRINCIPAL INVESTIGATOR: Richard R. Drake (Partnering PI: Alexander Parker)

CONTRACTING ORGANIZATION: Medical University of South Carolina
Charleston, SC 29425-8908

REPORT DATE: April 2013

TYPE OF REPORT: Annual Report

PREPARED FOR: U.S. Army Medical Research and Materiel Command
Fort Detrick, Maryland 21702-5012

DISTRIBUTION STATEMENT: Approved for Public Release;
Distribution Unlimited

The views, opinions and/or findings contained in this report are those of the author(s) and should not be construed as an official Department of the Army position, policy or decision unless so designated by other documentation.

REPORT DOCUMENTATION PAGE

Form Approved
OMB No. 0704-0188

1. REPORT DATE	2. REPORT TYPE	3. DATES COVERED
April 2013	Annual Report	1 April 2012 – 31 March 2013

4. TITLE AND SUBTITLE
Tissue and Metabolomic Biomarkers of Recurrent Renal Cell Carcinoma

5a. CONTRACT NUMBER
N/A

5b. GRANT NUMBER
W81XWH-10-1-0173

5c. PROGRAM ELEMENT NUMBER

6. AUTHOR(S)
Richard R. Drake, Ph.D.

E-Mail: draker@musc.edu

5d. PROJECT NUMBER
N/A

5e. TASK NUMBER
N/A

5f. WORK UNIT NUMBER
N/A

7. PERFORMING ORGANIZATION NAME(S) AND ADDRESS(ES)

Medical University of South Carolina

Charleston, SC 29425-8908

8. PERFORMING ORGANIZATION REPORT NUMBER
N/A

9. SPONSORING / MONITORING AGENCY NAME(S) AND ADDRESS(ES)
U.S. Army Medical Research and Materiel Command
Fort Detrick, Maryland 21702-5012

10. SPONSOR/MONITOR'S ACRONYM(S)
N/A

11. SPONSOR/MONITOR'S REPORT NUMBER(S)
N/A

12. DISTRIBUTION / AVAILABILITY STATEMENT
Approved for Public Release; Distribution Unlimited

13. SUPPLEMENTARY NOTES

14. ABSTRACT
The purpose of the study was to harness cutting-edge metabolomic and proteomic biomarker discovery technologies to identify novel biomarkers for ccRCC aggressiveness in primary tumor samples excised during surgery. Fresh-frozen tissue samples from 25 intermediate risk ccRCC patients who experienced progression to metastasis within 3 years of surgery and 25 intermediate risk ccRCC patients who remain progression free after 5 years of follow-up were be evaluated by MALDI mass spectrometry based tissue imaging and metabolomic profiling at Metabolon, Inc. This data has also been extended using new analysis workflows developed at MUSC using the high resolution MALDI-FTICR instrument to analyze lipid and glycan species directly on tissue. An emphasis on examining the molecular changes at the tumor margin interface has also been implemented. These latter methods are currently unique to MUSC and were developed specifically for this project. The cumulative data is currently being analyzed with the clinical data in the partnering PIs facility.

15. SUBJECT TERMS
Kidney cancer, biomarkers, metabolomics, MALDI imaging

16. SECURITY CLASSIFICATION OF:			17. LIMITATION OF ABSTRACT	18. NUMBER OF PAGES	19a. NAME OF RESPONSIBLE PERSON
a. REPORT	b. ABSTRACT	c. THIS PAGE			USAMRMC
U	U	U	UU	7	19b. TELEPHONE NUMBER *(include area code)*

Table of Contents

Page

W81XWH-10-1-0173: Tissue and Metabolomic Biomarkers of Recurrent Renal Cell Carcinoma

Partnering Investigators: Richard R. Drake, Ph.D. and Alexander S. Parker, Ph.D.

Annual Report from April 1, 2012 to March 30, 2013 for Drake at MUSC

Note: The time period from the last report, June 30, 2011 to March 30, 2012 was not active due to the grant transfer process.

Introduction: The incidence and mortality rates for renal cell carcinoma (RCC) have risen steadily for more than 30 years, with a poor 5-year survival rate and a characteristically unpredictable clinical course for the most common clear cell form (ccRCC). The primary treatment for patients with localized ccRCC is surgical excision, which can be highly effective for early stage cancers. However, due to lack of any early detection strategies, approximately 35-40% of patients with no evidence of metastasis at the time of surgery will subsequently experience metastatic progression. Two key clinical issues are the need to 1) identify ways of more accurately predicting which patients will experience metastatic progression following surgery for localized ccRCC and 2) develop new treatments that can be used in combination with surgical excision to reduce progression. The overall goal of our proposed study is to improve our understanding of the underlying mechanisms of clear cell RCC progression and enhance the ability to accurately predict which patients are at greatest risk of progression following surgery. We hypothesize that identification of specific tumor associated proteins directly in histopathological specimens and their corresponding metabolite profile can be linked with our existing panel of biomarkers of clear cell RCC aggressiveness to develop a novel biomarker-based prognostic nomogram/scoring system that can significantly improve the ability to accurately identify individuals most at risk of ccRCC progression following surgery. Four experimental Specific Aims are proposed as follows: **1.** To harness cutting-edge metabolomic and proteomic biomarker discovery technologies to identify novel biomarkers for ccRCC aggressiveness in primary tumor samples excised during surgery; **2.** Combine novel biomarkers from SA1 with existing panel of seven previously published biomarkers of ccRCC aggressiveness to develop composite biomarker-based algorithm for predicting progression following surgery for ccRCC; **3.** To harness cutting-edge metabolomic and proteomic biomarker discovery technologies to identify novel biomarkers that are differentially expressed in paired samples of primary and metastatic ccRCC; and **4.** To independently validate the differential expression of the candidate biomarkers identified in SA3 and estimate the association of the expression of these biomarkers in metastatic ccRCC with time to death. To accomplish this, fresh-frozen tissue samples from 25 intermediate risk ccRCC patients who experienced progression to metastasis within 3 years of surgery and 25 intermediate risk ccRCC patients who remain progression free after 5 years of follow-up will be evaluated by MALDI mass spectrometry based tissue imaging and metabolomic profiling. Also, the same tissue imaging and metabolomic approaches will be applied to fresh-frozen tissue samples from 15 patients with matched primary ccRCC tumor and metastatic lung ccRCC tumor pairs. A novel biomarker-based scoring algorithm for predicting ccRCC progression using a cohort of 1,500 patients undergoing nephrectomy for localized ccRCC will also be developed. An additional 250 patients

who have archived tumor blocks available from both primary and metastatic ccRCC will also be evaluated for development of a biomarker panel. For impact, the identification of molecular biomarkers within tumor tissue that correlate with risk of ccRCC progression has the potential to not only improve prognostic assessment and enhance post-operative surveillance, but also to inform on the underlying biology of ccRCC aggressiveness as well as to provide rational targets and strategies for therapeutic intervention.

Body: In the Statement of Work for this project, 7 Tasks were proposed over a three year period. The first three Tasks were proposed to be completed within the first 18 months of the project. Overall, excellent progress has been made on these Tasks, and no changes in the last Statement of Work (revised with the move to MUSC) and/or research directions are expected. The scientific progress for completion of three tasks involving the Drake laboratory are summarized, followed by a data example summary in the Appendix Materials.

Task 1. **Identify differentially expressed proteomic biomarkers by MALDI mass spectrometry imaging in a cohort of patients with localized ccRCC classified as being at intermediate risk for recurrence (i.e. progression to metastasis) following surgery.**

a. Perform MALDI-TOF MS imaging analysis of 50 ccRCC tissues classified as intermediate risk for recurrence; 25 that experienced recurrence within 3 years of surgery, and 25 that remain recurrence free > 5 years following surgery..
b. Analyze peak intensity data inter- and intra-sample to determine differentially expressed proteins and peptides.

MILESTONE: Establish a panel of 5-10 differentially expressed peak markers that distinguish intermediate risk ccRCC patients who experience progression to metastasis following surgery from intermediate risk ccRCC patients who do not experience progression to metastasis. Months 1-18 (Drake)

Experimental Progress: This task was initiated by Dr. Parker with the selection of 50 frozen ccRCC samples from the biorepository at Mayo Clinic. Samples from patients with non-recurrent disease were selected from individuals with no evidence of disease 5 years after surgery for ccRCC. Samples from patients with recurrent disease were selected from individuals who had detectable metatstatic ccRCC within three years of primary nephrectomy. In addition, samples were matched in pairs to age, race, gender, and pathology information. These samples were dehydrated in ethanol and sprayed with CHCA matrix, followed by tissue imaging in the UltraFlex III MALDI-TOF/TOF instrument (Bruker Daltonics). Following reading of each slide by a pathologist (Dr. Dean Troyer, at EVMS), regions of non-necrotic tumor were selected as regions of interest (ROIs) for selection of spectra. On average, 50-100 individual spectra per ROI were selected. As summarized from the original Year 1 report, usable spectra for 22 recurrent ccRCC and 26 non-recurrent ccRCC samples were obtained. These procedures and experiments cumulatively took approximately 10 months to complete, and represent a total of 48 ccRCC and 10 normal matched renal tissues. Since June 2011, the data analysis of the obtained ROI spectra for each sample was done using FlexAnalysis and FlexImaging software (from Bruker Daltonics). Tandem mass spectrometry of 10 tissues was also done to correlate protein peaks identified in the MALDI imaging data to small proteins/peptides. This has facilitated identification of thymosin beta 4, thymosin beta 10, S100 A8, S100A9, S100A11 as clear

markers distinguishing tumor from normal tissues. This task is essentially complete for the protein analysis aspects in the laboratory. The data analysis continues with Dr. Parker for other molecular correlates (as in Task 3). There are 24 peak candidates that are being assessed (see Table summary in Appendix).

Task 2. **Identify differentially expressed metabolite biomarkers in the same ccRCC tissue intermediate risk cohort described in Task 1.**

a. Perform metabolite analysis of 50 ccRCC tissues classified as intermediate risk for recurrence; 25 that experienced a recurrence within 3 years of surgery, and 25 that remain recurrence free > 5years following surgery.
b. Determine any differentially expressed metabolites reflective of disease recurrence and/or non-recurrence.

MILESTONE: Determine a panel of ccRCC metabolites (15-20) to predict disease recurrence at the time of surgery. Months 9-15 (Metabolon, Parker)

Experimental Progress: For this task, metabolite analysis is contracted to Metabolon, Inc, which provided initial requirements for tissue preparation. As indicated in Task 1, the tissue slices for analysis of metabolites were prepared at the time of MALDI slide preparation. Tumor tissues (approx 25 mg/sample) were sent frozen to Metabolon in month 9 of the project, and the negotiated analysis costs already paid to the company. Dr. Parker and Dr. Drake were subsequently informed by Metabolon that at least 50 mg, and preferably 100 mg, of tissue from each sample will give the best results. Subsequently, larger amounts of RCC tissue samples were sent to Metabolon in the Fall of 2012 and analysis was completed in December 2012. The analysis report was attached with Dr. Parker's last annual report, and is not included in this report. In the past few months this summer (June/July 2013), a subset of the tissues analyzed by Metabolon have been examined by MALDI imaging, with an emphasis on determining the distribution of differentially expressed phospholipid and small metabolite biomolecules from the Metabolon report. Examples are provided in the Appendix.

Task 4. **Identify differentially expressed proteomic biomarkers by MALDI mass spectrometry imaging in primary ccRCC tumor tissues matched to ccRCC tissue metastatic to the lung from the same person.**

a. Perform MALDI-TOF MS imaging analysis of 15 pairs of primary and metastatic renal tissues (30 total)
b. Analyze peak intensity data inter- and intra-sample to determine differentially expressed proteins and peptides

MILESTONE: Establish a panel of 5-10 differentially expressed peak markers that distinguish the primary and metastatic tumor pairs. Months 20-36 (Drake) To be done at MUSC

Experimental Progress: Dr. Parker has been trying to obtain these tissues from the Mayo Clinic Rochester, with little success. At the time of submission, these samples were available. Subsequent issues related to consent and permitted use of this specific sample cohort have precluded getting them for the proposed analyses. In the interim, we have begun analysis of 20

RCC tissues from recurrent and non-recurrent tumors, but tissues that contain extensive regions of tumor, margin areas and adjacent non-tumor regions. These tissues are being provided by longtime collaborator Dean Troyer, M.D., a GU pathologist at EVMS. Matched primary and metastatic tumor pairs are also being obtained from EVMS, from Dr. Troyer and the urologic surgeon there, Ray Lance, M.D. An emphasis on lipid and glycan analysis has been done.

Our preliminary studies have identified multiple glycan and glycoprotein species uniquely expressed in the tumor margin regions, but not expressed in the non-tumor or tumor regions of the same tissue. This is the result of using a novel method to profile N-linked glycans directly on tissue using MALDI-MS imaging following PNGaseF digests. Depending on the tissue, 30-40 N-glycan species can be simultaneously detected by this method. Individual glycan and/or lipid ion intensities are converted to a color pixel scale for creating an image, linked directly to the histopathology of the tissue. Using the unique tumor/margin RCC tissues, four patterns of N-glycan and lipid specie expression have been observed, those present in: 1) the immediate margin area of non-tumor tissue adjacent to tumor; 2) only in non-tumor regions; 3) only in tumor regions; or 4) primarily in tumor regions but extended beyond the margin. An initial analysis of glycoproteins present in these three regions has also been done using new HCD-PD-ETD glycopeptide sequencing workflows. We hypothesize that optimization of this experimental workflow can be used to identify specific glycoprotein and glycan biomarkers indicative of the many changes that occur during the transition of organ confined tumors to the metastatic phenotype. Target molecules, including proteins, will be further analyzed in the primary tumor and metastatic disease pairs. Examples of this data are provided in the Appendix section.

Key Research Accomplishments, Year 3 of the project:

1. Successful MALDI-MS imaging analysis of 68 renal tissue samples obtained from the Mayo Clinic, and an additional 20 tissues with tumor/margin/non-tumor regions from Eastern Virginia Medical School (via Dean Troyer, M.D.).

2. Established an optimized frozen ccRCC tissue preparation protocol with Mayo Clinic suitable for MALDI MS imaging and metabolomic analyses.

3. Identification of 38 candidate m./z protein peaks that are differentially expressed in recurrent ccRCC or non-recurrent ccRCC tissues.

4. Tentative identification of thymosin beta family peptides and S100 family member proteins as being differentially expressed in recurrent ccRCC tumors.

5. Established MALDI MS imaging methods to effectively profile the distribution of N-linked glycans, ceramides, sphingomyelins, phospholipids and small molecule metabolites.

Reportable Outcomes: There are no manuscripts submitted or published from this work, but one is invited for submission in September 2013 as part of a conference special issue in *Proteomics*. A paper describing the imaging of N-glycans in tissues, including renal tissues, has been submitted and is currently undergoing review for *Analytical Chemistry*. However, 4 oral presentations and 2 abstracts were presented at scientific meetings in the past year, as indicated below. An R21 grant to NCI/NIH targeting the margin glycoproteins in RCC has been submitted and is currently under review.

Oral presentations:

“Protein and Lipid Profiling of Recurrent and Non-Recurrent Renal Cell Carcinoma” Ourense Conference on Imaging Mass Spectrometry, Ourense, Spain, Sept. 2012

“MALDI Mass Spectrometry Imaging for On-Tissue Spatial Profiling of N-linked Glycans in Tumor Tissues.” Mass Spectrometry Applications to the Clinical Laboratory Annual Meeting, San Diego, CA, February 2013.

”Differential Molecular Profiling of Lipids and Glycans at the Tumor Margin of Clear Cell Renal Carcinoma Tissues by MALDI-MS Imaging.” American Society of Mass Spectrometry Annual Meeting, Minneapolis, MN, June 2013.

“Novel on-tissue glycosidase and lipase digestion workflows to identify complex glycan and lipid species by MALDI-TOF MS imaging.” Bruker Daltonics User Meeting, one of 9 invited speakers, ASMS Annual Meeting, Minneapolis, MN, June 2013.

Poster presentations:
“Defining the Molecular Tumor Margin Regions of Clear Cell Renal Carcinoma Tissues by MALDI-MS Imaging of Lipid and Glycan Species.” Genetourinary Cancer Symposia, American Society of Clinical Oncology, Orlando, FL, February 2013.

“MALDI mass spectrometry imaging for on-tissue spatial profiling of tumor-specific N-linked glycans and lipids in renal carcinomas.” American Association of Cancer Research Annual Meeting, Washington, DC, April 2013.

Conclusions: We have developed a combined proteomics, metabolomics, lipidomic and glycomic workflow to analyze recurrent and non-recurrent RCC tissues. We expect to submit multiple publications derived from this research, as well as several new grant applications.

Appendix Material:

Task 1 Data (since June 2011). The 24 potentially diagnostic peptide/protein peaks from the tissue profiling are listed in the two tables below, either as diagnostic for distinguishing tumor from non-tumor, or recurrent from non-recurrent disease.

	2789.31	4020.57	4057.1	4902.29	5322.25	6677.34	6803.89	7358.81	7888.64	7994.5	8180.67	8518.97
Tumor v Normal (p-val)	0.492188	0.013672	0.027344	0.019531	0.027344	0.322266	0.193359	0.009766	0.048828	0.625	0.193359	0.160156
Predicting Tumor												
AUC	0.59	0.78	0.79	0.71	0.77	0.48	0.58	0.83	0.79	0.58	0.64	0.64
avg normal	3.397607	5.440402	5.273798	4.125764	6.718046	9.180451	5.468302	2.89322	2.00293	2.329145	1.815883	1.409771
avg tumor	2.979012	3.425946	3.078513	33.2938	2.326152	20.12344	9.80114	1.310392	4.063745	2.745435	1.533707	1.32208
flipped ROC?	Yes	Yes	Yes	No	Yes	No	No	Yes	No	No	Yes	Yes
Recurrent v Nonrecurrent (p-val)	0.037109	0.695313	0.322266	1	0.275391	0.001953	0.001953	0.322266	0.556641	0.009766	0.013672	0.005859
Predicting Recurrent												
AUC	0.83	0.52	0.6	0.52	0.63	0.97	0.96	0.65	0.47	0.88	0.82	0.95
avg nonrecurrent	2.373837	4.236184	3.742605	7.496023	6.182317	27.70082	13.65414	2.665348	3.575228	3.542243	2.096156	1.775164
avg recurrent	4.002781	4.630164	4.609706	29.92355	2.861881	1.603072	1.615298	1.538265	2.491447	1.532337	1.253434	0.956688
flipped ROC?	No	No	No	No	Yes	Yes	Yes	Yes	Yes	Yes	Yes	Yes

	8535.84	8915.22	9251.5	9399.71	9564.38	9707.84	9899.12	10452.97	11072.09	11892.6	12717.29	13916.42
Tumor v Normal (p-val)	0.769531	0.083984	0.921875	0.027344	0.105469	1	0.921875	1	0.556641	0.695313	0.037109	0.625
Predicting Tumor												
AUC	0.53	0.63	0.43	0.79	0.65	0.54	0.5	0.52	0.55	0.5	0.69	0.49
avg normal	1.457491	2.242799	1.296484	1.77485	2.300889	1.757034	1.708495	1.478636	1.223314	1.080923	1.126007	3.599126
avg tumor	1.585021	1.500818	1.504389	1.294279	1.754914	1.755304	1.707063	1.439573	1.261293	1.026722	0.849875	6.031863
flipped ROC?	No	Yes	No	Yes	Yes	Yes	Yes	Yes	No	Yes	Yes	No
Recurrent v Nonrecurrent (p-val)	0.001953	0.001953	0.048828	0.083984	0.001953	0.001953	0.037109	0.013672	0.001953	0.005859	0.001953	0.001953
Predicting Recurrent												
AUC	0.95	1	0.73	0.72	0.98	0.91	0.82	0.92	0.99	0.85	0.94	0.95
avg nonrecurrent	1.969059	2.815659	0.99373	1.807804	3.146541	2.381502	2.184825	2.017273	1.790624	1.410884	1.39522	1.645536
avg recurrent	1.073453	0.927958	1.807143	1.261325	0.909262	1.130836	1.230732	0.900935	0.693983	0.696761	0.580663	7.985453
flipped ROC?	Yes	Yes	No	Yes	Yes	Yes	Yes	Yes	Yes	Yes	Yes	No

Tissues from 5 recurrent (tumor/normal matched) and 5 non-recurrent (tumor/normal matched) RCC specimens were homogenized and digested with trypsin for subsequent LC-MS/MS analysis on a Thermo LTQ MS platform. The resulting protein IDs, averaged per condition for normalized spectral counts per protein hit, for peptides under 20 kDa are presented. These match the mass range of the MALDI analysis that was done on the same tissues. The list is attached on the next page.

Task 4 Data (since July 2011):

Our group has been recently optimized and described a tissue profiling MALDI-IMS approach to uniquely profile the expression and distribution of N-glycans released by on-tissue PNGaseF digestions. Using mouse brains as a model system, generally 30-40 native glycans can be detected by MALDI-FT-ICR analysis. Confirmation of glycan structures were done using a combination of off-tissue permethylation and MALDI profiling, normal phase HPLC and exoglycosidase digests, all compared to existing glycan databases provided by the Consortium for Functional Glycomics. This data has recently been accepted pending formatting and clarification revisions to be published in *Analytical Chemistry*. This is a technique that was developed exclusively in the Drake laboratory. A summary of MALDI IMS and the PNGaseF tissue analysis workflow are provided in the schematics below.

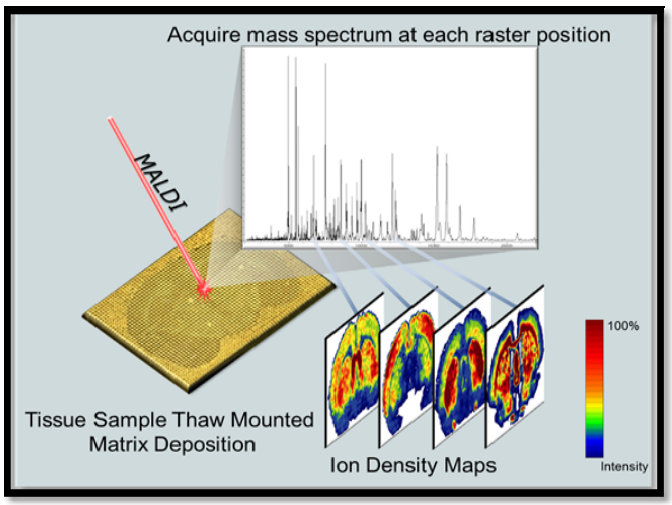

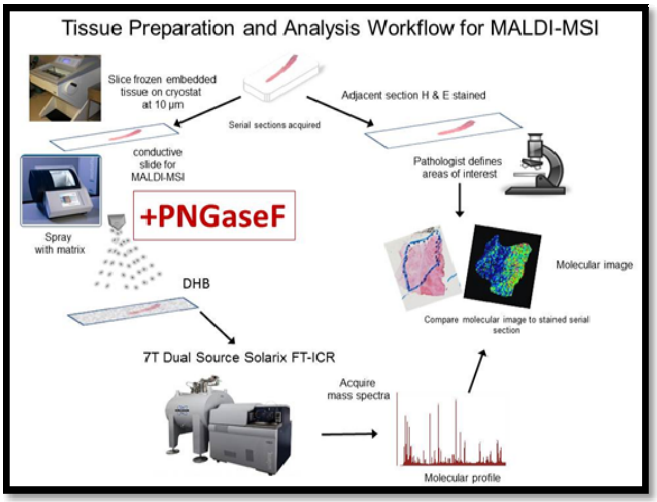

			Normalized Spectral counts			
Sequence Id	Description	Avg MW	avg normal	avg tumor	avg nonrecurrent	avg recurrent
P09668	CATH_HUMAN Pro-cathepsin H OS=Homo sapiens GN=CTSH PE=1 SV=4	848.88	1.82	0.00	0.64	1.19
P63313	TYB10_HUMAN Thymosin beta-10 OS=Homo sapiens GN=TMSB10 PE=1 SV	4894.48	2.18	4.90	4.42	2.66
P62328	TYB4_HUMAN Thymosin beta-4 OS=Homo sapiens GN=TMSB4X PE=1 SV=	4921.46	4.79	7.43	6.92	5.30
P59665	DEF1_HUMAN Neutrophil defensin 1 OS=Homo sapiens GN=DEFA1 PE=1	6306.36	2.57	4.01	1.87	4.71
P14406	CX7A2_HUMAN Cytochrome c oxidase subunit 7A2, mitochondrial OS=H	6721.81	1.65	0.48	0.96	1.17
P62987	RL40_HUMAN Ubiquitin-60S ribosomal protein L40 OS=Homo sapiens GN	8564.84	4.13	5.39	5.09	4.44
P02652	APOA2_HUMAN Apolipoprotein A-II OS=Homo sapiens GN=APOA2 PE=1	8707.91	2.83	2.61	2.80	2.65
P07602	SAP_HUMAN Proactivator polypeptide OS=Homo sapiens GN=PSAP PE=1	9107.55	3.30	2.16	2.29	3.17
O00483	NDUA4_HUMAN NADH dehydrogenase [ubiquinone] 1 alpha subcomple	9369.86	1.11	0.05	0.37	0.79
P14854	CX6B1_HUMAN Cytochrome c oxidase subunit 6B1 OS=Homo sapiens GN	10061.2	5.02	1.01	2.34	3.69
P10606	COX5B_HUMAN Cytochrome c oxidase subunit 5B, mitochondrial OS=Ho	10613.04	2.26	0.69	1.33	1.62
P61604	CH10_HUMAN 10 kDa heat shock protein, mitochondrial OS=Homo sapie	10800.5	5.99	3.76	5.31	4.43
P05109	S10A8_HUMAN Protein S100-A8 OS=Homo sapiens GN=S100A8 PE=1 SV=	10834.51	1.36	3.13	2.46	2.03
P60903	S10AA_HUMAN Protein S100-A10 OS=Homo sapiens GN=S100A10 PE=1 SV	11071.91	1.36	1.75	1.59	1.52
P62805	H4_HUMAN Histone H4 OS=Homo sapiens GN=HIST1H4A PE=1 SV=2	11236.15	16.43	16.61	18.08	14.96
P0CG05	LAC2_HUMAN Ig lambda-2 chain C regions OS=Homo sapiens GN=IGLC2 F	11294	4.23	4.41	3.55	5.09
P01834	IGKC_HUMAN Ig kappa chain C region OS=Homo sapiens GN=IGKC PE=1 S	11609	32.36	32.27	29.40	35.23
P31949	S10AB_HUMAN Protein S100-A11 OS=Homo sapiens GN=S100A11 PE=1 SV	11609.25	3.34	4.29	4.10	3.53
P35754	GLRX1_HUMAN Glutaredoxin-1 OS=Homo sapiens GN=GLRX PE=1 SV=2	11644.55	2.67	1.86	1.98	2.56
P61769	B2MG_HUMAN Beta-2-microglobulin OS=Homo sapiens GN=B2M PE=1 SV	11731.17	0.72	0.73	0.42	1.03
P01620	KV302_HUMAN Ig kappa chain V-III region SIE OS=Homo sapiens PE=1 SV	11775	1.60	2.15	1.68	2.07
P62942	FKB1A_HUMAN Peptidyl-prolyl cis-trans isomerase FKBP1A OS=Homo sa	11819.51	1.00	1.60	1.50	1.09
P61457	PHS_HUMAN Pterin-4-alpha-carbinolamine dehydratase OS=Homo sapie	11868.41	1.31	0.85	1.18	0.99
P80748	LV302_HUMAN Ig lambda chain V-III region LOI OS=Homo sapiens PE=1 S	11935	0.73	1.25	1.31	0.68
P84090	ERH_HUMAN Enhancer of rudimentary homolog OS=Homo sapiens GN=E	12127.74	0.47	0.95	0.96	0.47
Q9NZ45	CISD1_HUMAN CDGSH iron-sulfur domain-containing protein 1 OS=Hom	12199.05	0.57	0.84	0.38	1.04
P14174	MIF_HUMAN Macrophage migration inhibitory factor OS=Homo sapiens	12345.11	7.42	9.49	9.39	7.51
P01742	HV101_HUMAN Ig heavy chain V-I region EU OS=Homo sapiens PE=1 SV=	12472	1.35	1.99	1.58	1.77
P20674	COX5A_HUMAN Cytochrome c oxidase subunit 5A, mitochondrial OS=Ho	12501.17	2.70	0.32	1.28	1.74
P58546	MTPN_HUMAN Myotrophin OS=Homo sapiens GN=MTPN PE=1 SV=2	12763.6	2.04	2.29	2.40	1.93
P06702	S10A9_HUMAN Protein S100-A9 OS=Homo sapiens GN=S100A9 PE=1 SV=	13110.8	1.21	1.80	1.38	1.62
Q16718	NDUA5_HUMAN NADH dehydrogenase [ubiquinone] 1 alpha subcomple	13327.5	0.83	0.00	0.16	0.67
P14927	QCR7_HUMAN Cytochrome b-c1 complex subunit 7 OS=Homo sapiens GI	13399.26	0.94	0.16	0.58	0.52
Q71UI9	H2AV_HUMAN Histone H2A.V OS=Homo sapiens GN=H2AFV PE=1 SV=3	13508.69	1.15	0.99	0.89	1.25
O75348	VATG1_HUMAN V-type proton ATPase subunit G 1 OS=Homo sapiens GN	13626.33	2.35	0.42	0.90	1.87
Q13510	ASAH1_HUMAN Acid ceramidase OS=Homo sapiens GN=ASAH1 PE=1 SV=	13704.97	1.36	0.85	0.91	1.30
P02766	TTHY_HUMAN Transthyretin OS=Homo sapiens GN=TTR PE=1 SV=1	13761.41	6.71	5.41	5.54	6.58
P62807	H2B1C_HUMAN Histone H2B type 1-C/E/F/G/I OS=Homo sapiens GN=HIS	13774.95	3.11	3.63	3.51	3.23
P33778	H2B1B_HUMAN Histone H2B type 1-B OS=Homo sapiens GN=HIST1H2BB	13819	16.73	18.99	16.74	18.98
P20671	H2A1D_HUMAN Histone H2A type 1-D OS=Homo sapiens GN=HIST1H2AD	13976.29	4.24	5.19	5.11	4.32
P04908	H2A1B_HUMAN Histone H2A type 1-B/E OS=Homo sapiens GN=HIST1H2A	14004.3	15.72	18.29	16.42	17.58
Q96A08	H2B1A_HUMAN Histone H2B type 1-A OS=Homo sapiens GN=HIST1H2BA	14036.31	8.11	8.26	8.29	8.08
Q96QV6	H2A1A_HUMAN Histone H2A type 1-A OS=Homo sapiens GN=HIST1H2AA	14102.32	10.80	16.16	14.66	12.31
A6NHG4	DDTL_HUMAN D-dopachrome decarboxylase-like protein OS=Homo sapi	14195.29	3.58	2.45	3.00	3.04
P07148	FABPL_HUMAN Fatty acid-binding protein, liver OS=Homo sapiens GN=F	14208.38	3.82	0.53	1.34	3.01
P52758	UK114_HUMAN Ribonuclease UK114 OS=Homo sapiens GN=HRSP12 PE=1	14362.49	5.37	2.88	4.02	4.23
P61916	NPC2_HUMAN Epididymal secretory protein E1 OS=Homo sapiens GN=N	14578.79	2.06	0.05	0.69	1.42
P09382	LEG1_HUMAN Galectin-1 OS=Homo sapiens GN=LGALS1 PE=1 SV=2	14584.51	6.13	10.45	9.08	7.49
P61626	LYSC_HUMAN Lysozyme C OS=Homo sapiens GN=LYZ PE=1 SV=1	14700.67	3.67	1.11	1.33	3.44
P05413	FABPH_HUMAN Fatty acid-binding protein, heart OS=Homo sapiens GN=	14726.84	3.50	2.42	3.66	2.25
O15540	FABP7_HUMAN Fatty acid-binding protein, brain OS=Homo sapiens GN=	14757.72	2.01	11.67	11.73	1.95
P07737	PROF1_HUMAN Profilin-1 OS=Homo sapiens GN=PFN1 PE=1 SV=2	14923.04	6.31	8.05	8.24	6.12
P30049	ATPD_HUMAN ATP synthase subunit delta, mitochondrial OS=Homo sap	15019.93	2.48	1.10	1.27	2.30
P69905	HBA_HUMAN Hemoglobin subunit alpha OS=Homo sapiens GN=HBA1 PE	15126.36	34.77	101.93	47.92	88.77
P00167	CYB5_HUMAN Cytochrome b5 OS=Homo sapiens GN=CYB5A PE=1 SV=2	15198.91	3.30	2.46	2.73	3.03
Q16695	H31T_HUMAN Histone H3.1t OS=Homo sapiens GN=HIST3H3 PE=1 SV=3	15377.06	4.89	6.71	6.95	4.65
O60361	NDK8_HUMAN Putative nucleoside diphosphate kinase OS=Homo sapie	15529.06	1.41	1.80	1.48	1.72
P00441	SODC_HUMAN Superoxide dismutase [Cu-Zn] OS=Homo sapiens GN=SO	15804.55	5.97	4.59	4.97	5.58
P68871	HBB_HUMAN Hemoglobin subunit beta OS=Homo sapiens GN=HBB PE=1	15867.22	148.25	372.74	191.86	329.14
P02042	HBD_HUMAN Hemoglobin subunit delta OS=Homo sapiens GN=HBD PE=	15924.29	9.81	16.43	11.86	14.38
P39019	RS19_HUMAN 40S ribosomal protein S19 OS=Homo sapiens GN=RPS19 PE	15929.31	0.26	0.85	0.54	0.58
P69892	HBG2_HUMAN Hemoglobin subunit gamma-2 OS=Homo sapiens GN=HBG	15995.25	0.35	0.93	0.21	1.08
P69891	HBG1_HUMAN Hemoglobin subunit gamma-1 OS=Homo sapiens GN=HBG	16009.28	3.55	12.93	2.52	13.96
P60660	MYL6_HUMAN Myosin light polypeptide 6 OS=Homo sapiens GN=MYL6 P	16798.86	8.22	7.91	8.59	7.53
P30044	PRDX5_HUMAN Peroxiredoxin-5, mitochondrial OS=Homo sapiens GN=P	17030.75	4.09	2.83	3.53	3.39
P13073	COX41_HUMAN Cytochrome c oxidase subunit 4 isoform 1, mitochondri	17199.8	1.85	0.64	1.23	1.26
Q9BVM4	A2LD1_HUMAN Gamma-glutamylaminecyclotransferase OS=Homo sapie	17328.59	1.52	0.22	0.80	0.93
P62937	PPIA_HUMAN Peptidyl-prolyl cis-trans isomerase A OS=Homo sapiens G	18012.49	20.10	19.98	21.07	19.01
Q9Y536	PAL4A_HUMAN Peptidyl-prolyl cis-trans isomerase A-like 4A/B/C OS=Ho	18181.8	1.58	1.60	1.87	1.31
O75947	ATP5H_HUMAN ATP synthase subunit d, mitochondrial OS=Homo sapier	18360.02	4.36	1.12	2.83	2.66
P23528	COF1_HUMAN Cofilin-1 OS=Homo sapiens GN=CFL1 PE=1 SV=3	18371.3	6.15	6.06	6.76	5.45
B9A064	IGLL5_HUMAN Immunoglobulin lambda-like polypeptide 5 OS=Homo sa	19278.73	6.77	6.54	6.15	7.16
P19105	ML12A_HUMAN Myosin regulatory light chain 12A OS=Homo sapiens GN	19794.13	1.89	1.53	1.85	1.57
P02792	FRIL_HUMAN Ferritin light chain OS=Homo sapiens GN=FTL PE=1 SV=2	19888.48	9.94	11.07	9.97	11.03
Q99497	PARK7_HUMAN Protein DJ-1 OS=Homo sapiens GN=PARK7 PE=1 SV=2	19891.05	4.76	2.97	3.79	3.94

MALDI Imaging of N-Glycans and Comparison to Histopathology. ccRCC tissues were cut at 10 µm and sequentially ethanol washed to remove lipids. PNGase F (20 mU) was applied using the Bruker ImagePrep, followed by a 2 Hr incubation at 37ºC. DHB matrix was then applied, prior to imaging. As a control, duplicate ccRCC tissues were analyzed with and without PNGase F treatment, then extracted in water for off-tissue profiling (**Fig 1A.**). A comparison of the mass spectra reveals robust differences between the PNGase F treated and non treated tissues, and further this is further illustrated in the glycan profile images linked to the H&E overlay for three representative glycans at m/z 2486, 2631 and 2059 (**Fig 1B.**). Each individual mass to charge ratio (m/z) can be queried for peak intensities in each spot analyzed. A color pixel scale is used to convert the intensities to a colar representation; hence an image of color intensity is generated for each m/z of interest.

Figure 1A.

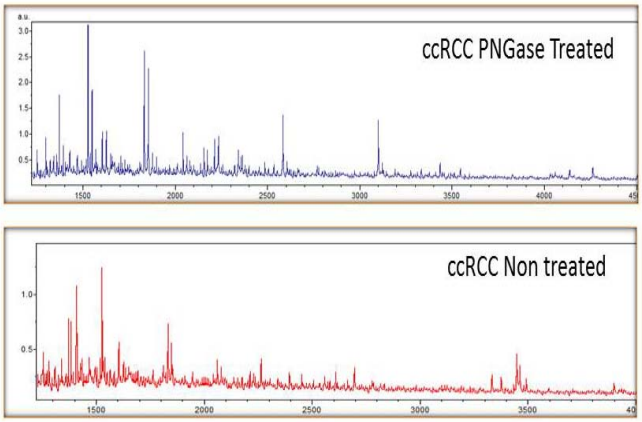

Figure 1B.

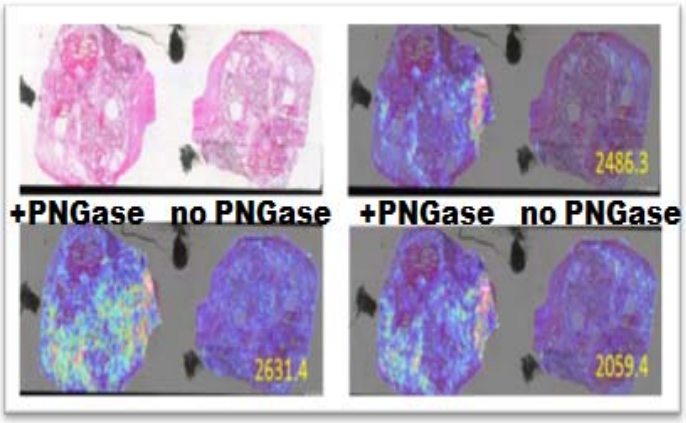

In the course of these initial analyses, it was observed that there were specific examples of glycans that were expressed in the margin region between tumor and non-tumor regions. This was further analyzed using larger tissue specimens specifically collected for that purpose, provided by Dr Dean Troyer, Eastern Virginia Medical School, and eight samples have already been analyzed for on-tissue PNGaseF digestions and MALDI-IMS. Representative profiles of one tissue is shown in the two panels below (Figure 2A/2B).

Figure 2A.

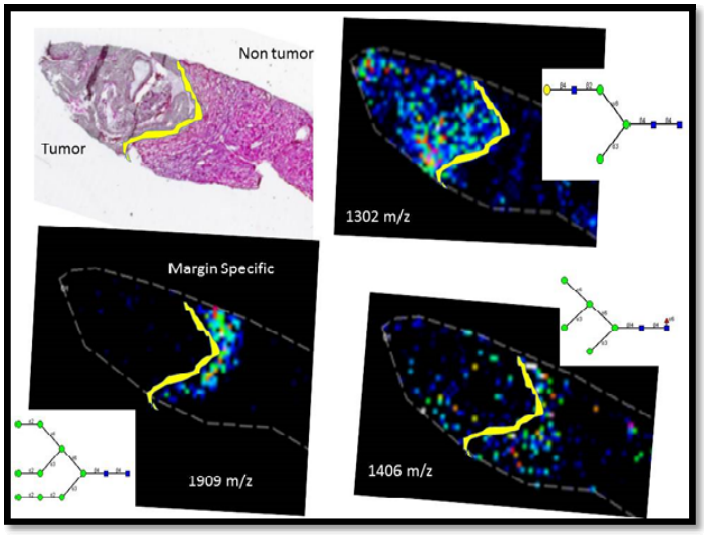

Figure 2B.

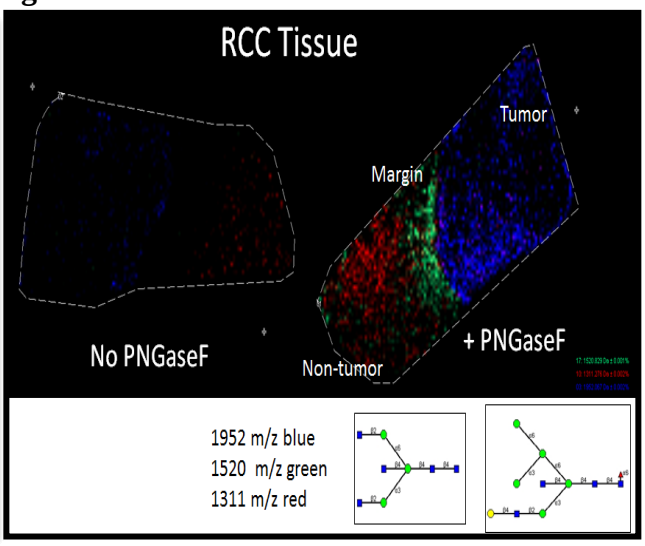

There are distinct glycosylation profiles between tumor, non-tumor and margin regions adjacent to the tumor. The yellow band along the margin was added to illustrate the boundary of the region.We have made glycan structure determinations based on accurate mass, databases and off-tissue analysis. Two examples of structural assignments following PNGase F on-tissue digest of an RCC tissue is shown in Figure 3A/3B. For both structures below, searches of the native mass CFG database, and comparison to permethylated glycans of extracted glycans from the same tissue. These two species represent distinct glycan species associated with expression, or lack thereof, at the margin interface of tumor and non-tumor regions.

Figure 3A

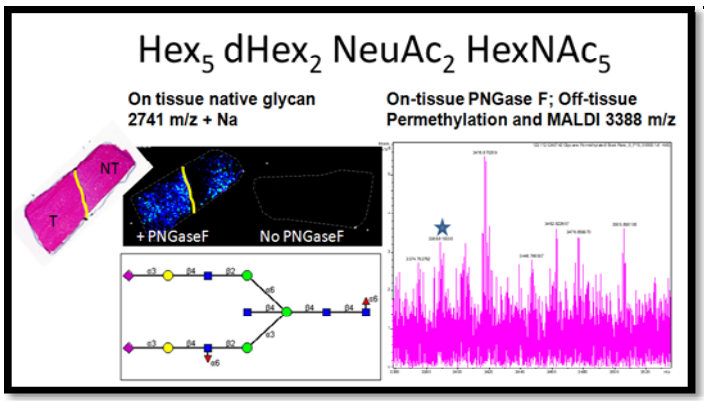

Figure 3B

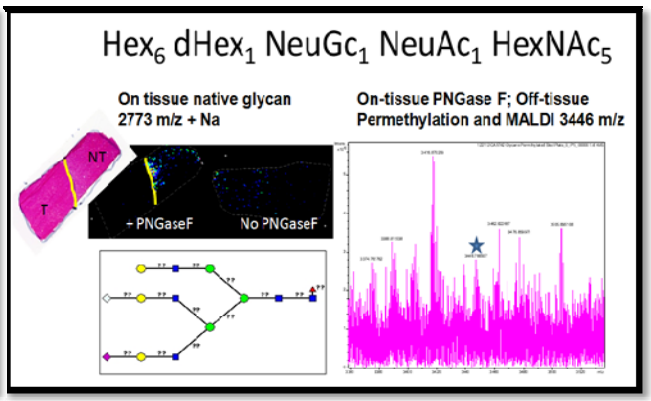

Preliminary Protein Analysis of Margin vs. Tumor and non-tumor regions. Because the margin glycan expression was so well defined, 1 mm slices were scraped from the margin region, and a similar scrape from tumor and non-tumor regions. Tissues were digested in TFE and

digested with tryspin, and analyzed by LC-MS for total protein composition. The Venn diagram (Figure 4A) summarizes the total number of proteins identified from each tissue region, and the table highlights several extracellular matrix proteins identified exclusively in the margin region (out of 228)(Figure 4B). This region is clearly distinct from the other two regions analyzed, and reflects protein differences consistent with an active EMT process. This baseline data will be used with the glycopeptide analyses described in Figure 5.

Figure 4A

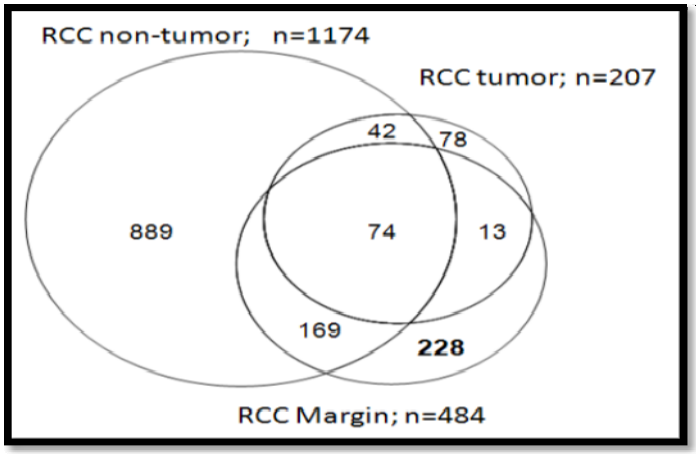

Figure 4B

Protein Name	# Unique Peptides	MASCOT score
Extracellular Matrix/ Adhesion/Junctions		
Protocadherin 17	3	56.5
Protocadherin 20	2	58.4
ADAMTS18	4	59.2
ADAMTS4	2	50.7
Integrin alpha-3	3	55.3
Neural Cell Adhesion Molecule L1	3	55.4
Laminin subunit gamma 3*	3	70.5
Fer like protein 5*	2	51.9
Synaptajanin-2	2	67.3
Vitronectin	2	50.2
Cubulin	3	79.4
Neurexin-1 beta*	3	54.9

HCD-PD-ETD Glycopeptide from RCC Tissue Example: In the past, MS-based glycoproteomic studies relied on the release of glycan moieties from glycopeptides followed by separate MS analysis of the glycans and the peptides. Recently, intact glycopeptide strategies are emerging

for use with high resolution Orbitrap instruments, typified by Higher-energy Collision Dissociation-Product Dependent-Electron Transfer Dissociation (HCD-PD-ETD). This method is a data-dependent acquisition, based on detection of glycan oxonium ions that trigger further analysis of the peptide carrier by ETD. An initial analysis of glycopeptides from the tumor region of one RCC tissue has been done, using a HILIC resin enrichment and HCD-PD-ETD protocol Glycopeptide data was obtained on a Thermo Orbitrap Elite mass spectrometer. In Figure 5 (below), a glycopeptide of receptor-type protein phosphastase beta was identified. The same glycan ion could also be detected in the glycan MALDI imaging profile of the same tumor tissue.

Figure 5.

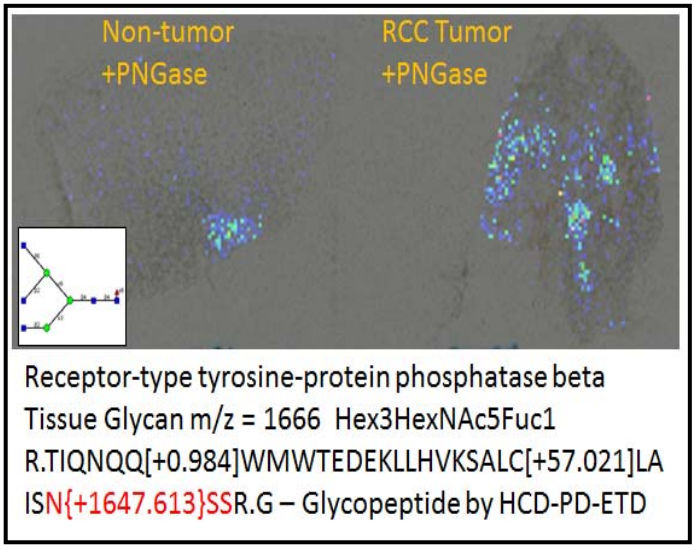

MALDI Imaging of Lipids and Comparison to Histopathology. ccRCC tissues (n=17) were cut at 10 µm, washed in water, dessicated and sprayed with DHB using an ImagePrep. Lipid images were obtained on a 7T Dual Source Solarix FT-ICR Mass spectrometer (Bruker Daltonics). Phosphatidylcholines, lyso-PCs, sphingomyelins and ceramides were profiled in positive ion mode. The image panel below in Figure 6 illustrates the type of distribution profiles that are obtained.

Figure 6.

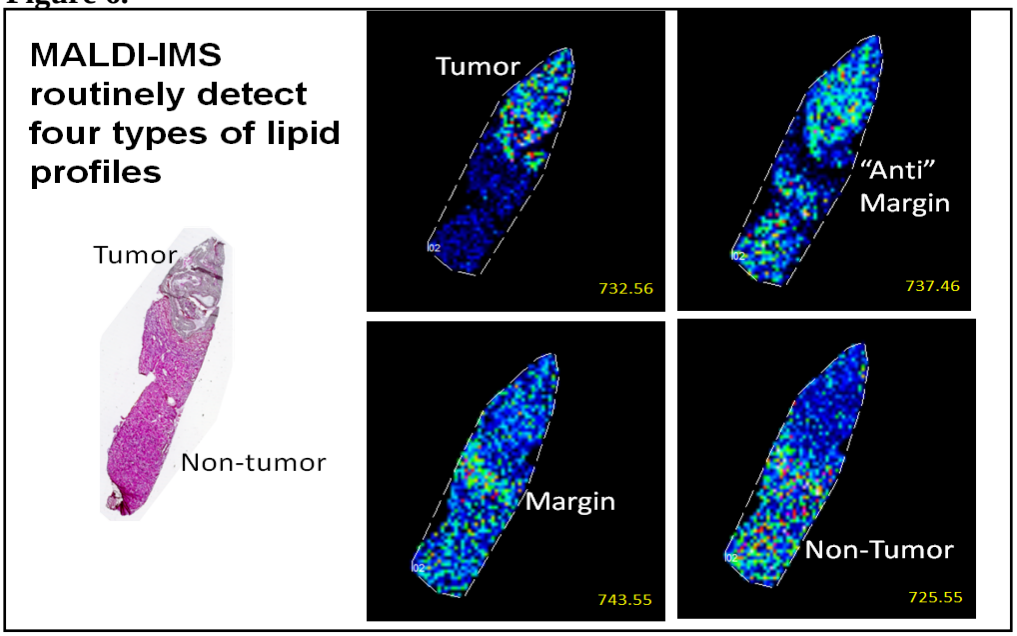

Lyso-PCs and other lipids with 1 or 2 double bonds in the fatty acid chains are associated with the presence of RCC. An example image of a Lyso-PC (C18:0) in non tumor tissues compared to a Lyso-PC (C18:1) is shown below in Figure 7.

Figure 7.

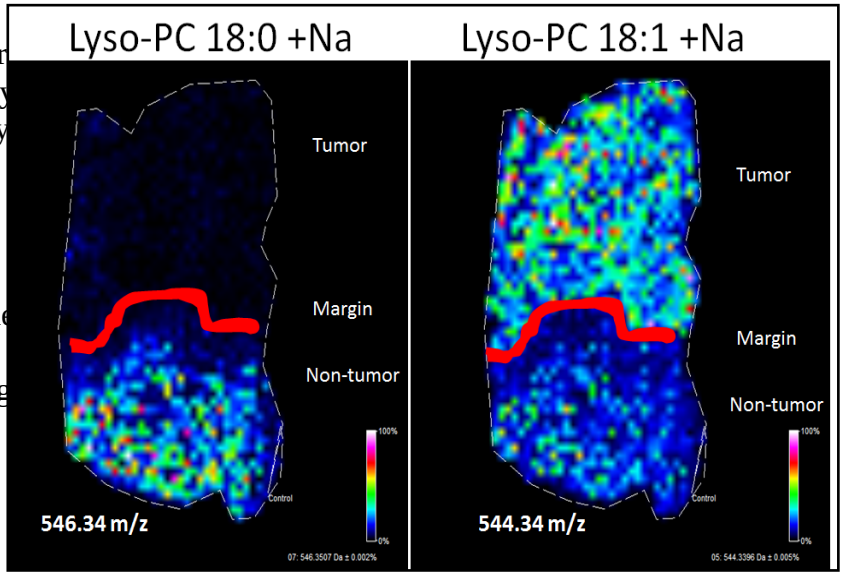

In the data summary shown in Figur 8 below, 30 lipid species detected by MALDI-imaging mass spectrometry in 17 RCC tissues are listed. Lipids differentially expressed in either tumor or normal in at least 14 of 17 sample pairs are listed. Representative images for two of the lipid species for normal or tumor expression are shown in the imaging panels on the right, with an overlay of the two expression profiles also included.

Figure 8.

m/z	Elevated in Normal
627.54	17
625.52	16
916.52	16
575.51	15
599.51	15
720.59	15
724.53	15
731.61	15
769.57	15
780.56	15
790.54	15
806.57	15
672.42	14
753.59	14
778.48	14
828.56	14

m/z	Elevated in Tumor
671.58	16
763.47	16
718.58	15
810.61	15
812.62	15
848.56	15
850.58	15
492.1	14
582.3	14
663.55	14
786.61	14
794.61	14
834.6	14
874.58	14

Out of 17 ccRCC tissues analyzed